Generation of biphoton correlation trains through spectral filtering

Joseph M. Lukens,[1] Ogaga Odele,[1] Carsten Langrock,[2] Martin M. Fejer,[2] Daniel E. Leaird,[1] and Andrew M. Weiner[1],*

[1]*School of Electrical and Computer Engineering, Purdue University, West Lafayette, Indiana 47906, USA*

[2]*E. L. Ginzton Laboratory, Stanford University, Stanford, California 94305, USA*

*amw@purdue.edu

Abstract: We demonstrate the generation of two-photon correlation trains based on spectral filtering of broadband biphotons. Programmable amplitude filtering is employed to create biphoton frequency combs, which when coupled with optical dispersion allows us to experimentally verify the temporal Talbot effect for entangled photons. Additionally, an alternative spectral phase-filtering approach is shown to significantly improve the overall efficiency of the generation process when a comb-like spectrum is not required. Our technique is ideal for the creation of tunable and high-repetition-rate biphoton states.

OCIS codes: (270.0270) Quantum optics; (320.5540) Pulse shaping; (070.6760) Talbot and self-imaging effects.

References and links

1. J. Perina, Jr., "Characterization of a resonator using entangled two-photon states," Opt. Commun. **221**, 153–161 (2003).
2. Y. J. Lu, R. L. Campbell, and Z. Y. Ou, "Mode-locked two-photon states," Phys. Rev. Lett. **91**, 163602 (2003).
3. H. Goto, Y. Yanagihara, H. Wang, T. Horikiri, and T. Kobayashi, "Observation of an oscillatory correlation function of multimode two-photon pairs," Phys. Rev. A **68**, 015803 (2003).
4. H. Goto, H. Wang, T. Horikiri, Y. Yanagihara, and T. Kobayashi, "Two-photon interference of multimode two-photon pairs with an unbalanced interferometer," Phys. Rev. A **69**, 035801 (2004).
5. H. Wang, T. Horikiri, and T. Kobayashi, "Polarization-entangled mode-locked photons from cavity-enhanced spontaneous parametric down-conversion," Phys. Rev. A **70**, 043804 (2004).
6. H.-b. Wang and T. Kobayashi, "Quantum interference of a mode-locked two-photon state," Phys. Rev. A **70**, 053816 (2004).
7. M. A. Sagioro, C. Olindo, C. H. Monken, and S. Pádua, "Time control of two-photon interference," Phys. Rev. A **69**, 053817 (2004).
8. A. Zavatta, S. Viciani, and M. Bellini, "Recurrent fourth-order interference dips and peaks with a comblike two-photon entangled state," Phys. Rev. A **70**, 023806 (2004).
9. F.-Y. Wang, B.-S. Shi, and G.-C. Guo, "Observation of time correlation function of multimode two-photon pairs on a rubidium D_2 line," Opt. Lett. **33**, 2191–2193 (2008).
10. W. C. Jiang, X. Lu, J. Zhang, O. Painter, and Q. Lin, "A silicon-chip source of bright photon-pair comb," arXiv:1210.4455 (2012).
11. A. Aspect, "Bell's inequality test: more ideal than ever," Nature **398**, 189–190 (1999).
12. N. Gisin and R. Thew, "Quantum communication," Nature Photon. **1**, 165–171 (2007).
13. T. Udem, R. Holzwarth, and T. W. Hänsch, "Optical frequency metrology," Nature **416**, 233–237 (2002).
14. N. R. Newbury, "Searching for applications with a fine-tooth comb," Nature Photon. **5**, 186–188 (2011).
15. S. Clemmen, K. P. Huy, W. Bogaerts, R. G. Baets, P. Emplit, and S. Massar, "Continuous wave photon pair generation in silicon-on-insulator waveguides and ring resonators," Opt. Express **17**, 16558–16570 (2009).
16. S. Azzini, D. Grassani, M. J. Strain, M. Sorel, L. G. Helt, J. E. Sipe, M. Liscidini, M. Galli, and D. Bajoni, "Ultra-low power generation of twin photons in a compact silicon ring resonator," Opt. Express **20**, 23100–23107 (2012).

#206479 - $15.00 USD Received 4 Mar 2014; revised 3 Apr 2014; accepted 6 Apr 2014; published 14 Apr 2014

17. Y. J. Lu and Z. Y. Ou, "Optical parametric oscillator far below threshold: experiment versus theory," Phys. Rev. A **62**, 033804 (2000).
18. V. Torres-Company, J. Lancis, H. Lajunen, and A. T. Friberg, "Coherence revivals in two-photon frequency combs," Phys. Rev. A **84**, 033830 (2011).
19. T. Jannson and J. Jannson, "Temporal self-imaging effect in single-mode fibers," J. Opt. Soc. Am. **71**, 1373–1376 (1981).
20. V. Torres-Company, J. Lancis, and P. Andrés, "Space-time analogies in optics," in *Progress in Optics*, E. Wolf ed., vol. 56, 1–80 (Elsevier, 2011).
21. A. M. Weiner, "Femtosecond pulse shaping using spatial light modulators," Rev. Sci. Instrum. **71**, 1929–1960 (2000).
22. A. M. Weiner, *Ultrafast Optics* (Wiley, Hoboken, NJ, 2009).
23. A. M. Weiner, "Ultrafast optical pulse shaping: a tutorial review," Opt. Commun. **284**, 3669 – 3692 (2011).
24. L. Mandel and E. Wolf, *Optical Coherence and Quantum Optics* (Cambridge University Press, Cambridge, UK, 1995).
25. Y. Shih, "Entangled biphoton source - property and preparation," Rep. Prog. Phys. **66**, 1009 (2003).
26. B. Dayan, A. Pe'er, A. A. Friesem, and Y. Silberberg, "Nonlinear interactions with an ultrahigh flux of broadband entangled photons," Phys. Rev. Lett. **94**, 043602 (2005).
27. A. Pe'er, B. Dayan, A. A. Friesem, and Y. Silberberg, "Temporal shaping of entangled photons," Phys. Rev. Lett. **94**, 073601 (2005).
28. F. Zäh, M. Halder, and T. Feurer, "Amplitude and phase modulation of time-energy entangled two-photon states," Opt. Express **16**, 16452–16458 (2008).
29. K. A. O'Donnell and A. B. U'Ren, "Time-resolved up-conversion of entangled photon pairs," Phys. Rev. Lett. **103**, 123602 (2009).
30. S. Sensarn, G. Y. Yin, and S. E. Harris, "Generation and compression of chirped biphotons," Phys. Rev. Lett. **104**, 253602 (2010).
31. K. A. O'Donnell, "Observations of dispersion cancellation of entangled photon pairs," Phys. Rev. Lett. **106**, 063601 (2011).
32. J. M. Lukens, A. Dezfooliyan, C. Langrock, M. M. Fejer, D. E. Leaird, and A. M. Weiner, "Demonstration of high-order dispersion cancellation with an ultrahigh-efficiency sum-frequency correlator," Phys. Rev. Lett. **111**, 193603 (2013).
33. K. R. Parameswaran, R. K. Route, J. R. Kurz, R. V. Roussev, M. M. Fejer, and M. Fujimura, "Highly efficient second-harmonic generation in buried waveguides formed by annealed and reverse proton exchange in periodically poled lithium niobate," Opt. Lett. **27**, 179–181 (2002).
34. C. Langrock, S. Kumar, J. E. McGeehan, A. E. Willner, and M. M. Fejer, "All-optical signal processing using $\chi^{(2)}$ nonlinearities in guided-wave devices," J. Lightwave Technol. **24**, 2579 (2006).
35. A. M. Weiner and D. E. Leaird, "Generation of terahertz-rate trains of femtosecond pulses by phase-only filtering," Opt. Lett. **15**, 51–53 (1990).
36. H. Talbot, "Facts relating to optical science." Philos. Mag. Ser. 3 **9**, 401–407 (1836).
37. K. Patorski, "The self-imaging phenomenon and its applications," in *Progress in Optics*, E. Wolf ed., vol. 27, 1–108 (Elsevier, 1989).
38. J. Wen, Y. Zhang, and M. Xiao, "The Talbot effect: recent advances in classical optics, nonlinear optics, and quantum optics," Adv. Opt. Photon. **5**, 83–130 (2013).
39. K.-H. Luo, J. Wen, X.-H. Chen, Q. Liu, M. Xiao, and L.-A. Wu, "Second-order Talbot effect with entangled photon pairs," Phys. Rev. A **80**, 043820 (2009).
40. X.-B. Song, H.-B. Wang, J. Xiong, K. Wang, X. Zhang, K.-H. Luo, and L.-A. Wu, "Experimental observation of quantum Talbot effects," Phys. Rev. Lett. **107**, 033902 (2011).
41. B. H. Kolner and M. Nazarathy, "Temporal imaging with a time lens," Opt. Lett. **14**, 630–632 (1989).
42. B. H. Kolner, "Space-time duality and the theory of temporal imaging," IEEE J. Quantum Electron. **30**, 1951–1963 (1994).
43. T. Yamamoto, T. Komukai, K. Suzuki, and A. Takada, "Spectrally flattened phase-locked multi-carrier light generator with phase modulators and chirped fibre Bragg grating," Electron. Lett. **43**, 1040–1042 (2007).
44. V. Torres-Company, J. Lancis, and P. Andrés, "Lossless equalization of frequency combs," Opt. Lett. **33**, 1822–1824 (2008).
45. J. Azaña and M. A. Muriel, "Technique for multiplying the repetition rates of periodic trains of pulses by means of a temporal self-imaging effect in chirped fiber gratings," Opt. Lett. **24**, 1672–1674 (1999).
46. J. Azaña and M. Muriel, "Temporal self-imaging effects: theory and application for multiplying pulse repetition rates," IEEE J. Sel. Top. Quantum Electron. **7**, 728–744 (2001).
47. J. Caraquitena, Z. Jiang, D. E. Leaird, and A. M. Weiner, "Tunable pulse repetition-rate multiplication using phase-only line-by-line pulse shaping," Opt. Lett. **32**, 716–718 (2007).
48. J. M. Lukens, D. E. Leaird, and A. M. Weiner, "A temporal cloak at telecommunication data rate," Nature **498**, 205–208 (2013).
49. J. D. Franson, "Nonlocal cancellation of dispersion," Phys. Rev. A **45**, 3126–3132 (1992).

#206479 - $15.00 USD Received 4 Mar 2014; revised 3 Apr 2014; accepted 6 Apr 2014; published 14 Apr 2014

50. I. Sizer, T., "Increase in laser repetition rate by spectral selection," IEEE J. Quantum Electron. **25**, 97–103 (1989).
51. P. Petropoulos, M. Ibsen, M. N. Zervas, and D. J. Richardson, "Generation of a 40-GHz pulse stream by pulse multiplication with a sampled fiber Bragg grating," Opt. Lett. **25**, 521–523 (2000).
52. K. Yiannopoulos, K. Vyrsokinos, E. Kehayas, N. Pleros, K. Vlachos, H. Avramopoulos, and G. Guekos, "Rate multiplication by double-passing Fabry-Perot filtering," IEEE Photon. Technol. Lett. **15**, 1294–1296 (2003).
53. A. M. Weiner, D. E. Leaird, G. P. Wiederrecht, and K. A. Nelson, "Femtosecond pulse sequences used for optical manipulation of molecular motion," Science **247**, 1317–1319 (1990).
54. M. R. Schroeder, *Number Theory in Science and Communication* (Springer-Verlag, Berlin, 1986).

1. Introduction

The pursuit of two-photon frequency combs—entangled photons occurring in a superposition of discrete spectral mode pairs [1–10]—offers much promise, as such biphotons have the potential to combine the unique characteristics of quantum entanglement [11, 12] with the precision of classical optical frequency comb metrology [13, 14]. Several configurations generating such photonic states have been implemented, including spontaneous four-wave mixing in microresonators [10, 15, 16], cavity-enhanced spontaneous parametric downconversion (SPDC) [2–5, 9, 17], and direct filtering of broadband biphotons [7, 8]. Assuming phase locking of the constituent spectral modes, the temporal correlation function of these biphoton frequency combs consists of a train of peaks, the number of which is approximately equal to the spectral mode spacing divided by the linewidth. Indirect measurements based on Hong-Ou-Mandel interference have revealed the periodic coincidence dips indicative of such correlation trains [2, 7, 8], and with sufficiently low repetition rates, direct correlation measurements have been made possible as well [3,5,9]. Moreover, it has been predicted theoretically [18] that propagation of these two-photon frequency combs through dispersive media will produce revivals of the temporal correlation function at discrete dispersion values, through an extension of the classical temporal Talbot effect [19, 20].

In this work, we experimentally examine a new method for generating biphoton correlation trains based on optical filtering with spatial light modulators [21–23]. Our technique permits the creation of extremely high-repetition-rate ($\sim$THz) trains, with programmable control of peak number and spacing. We explore both amplitude and phase filtering approaches, each with its own advantages. With amplitude filtering, we create coherent biphoton frequency combs with tunable properties and experimentally demonstrate the two-photon temporal Talbot effect for the first time. Alternatively, when the temporal phase of the biphoton wavepacket is unimportant, we show that spectral phase-only filtering can yield correlation trains with much greater efficiency, even though the filtered spectrum does not contain a series of discrete frequencies—i.e., it is not comb-like. Our results therefore not only contribute to the development of two-photon frequency combs, but also show that for some applications it may be possible to remove the requirement of a true frequency comb in favor of a low-loss spectral phase filter.

In Sec. 2 we introduce the experimental setup and describe the generation of a two-photon correlation train using amplitude filtering. We then manipulate this frequency comb in Sec. 3 to show the temporal Talbot effect. In Sec. 4 an alternative phase-only approach is implemented, which offers improved efficiency in correlation train production. Finally, we explore the limitations imposed by the spectral resolution of our pulse shaper in Sec. 5, concluding with a short summary of all findings in Sec. 6.

2. Amplitude filtering

The quantum state produced by degenerate SPDC of a continuous-wave pump at frequency $2\omega_0$ can be expressed as [24]

$$|\Psi\rangle = M|\text{vac}\rangle_s|\text{vac}\rangle_i + \int d\Omega\, \phi(\Omega)|\omega_0+\Omega\rangle_s|\omega_0-\Omega\rangle_i, \tag{1}$$

#206479 - $15.00 USD Received 4 Mar 2014; revised 3 Apr 2014; accepted 6 Apr 2014; published 14 Apr 2014

where $M \sim 1$, "vac" denotes the vacuum state, s the signal photon, and i the idler. Here we choose to distinguish signal and idler photons by frequency, with the former denoting the high-frequency photon and the latter the low-frequency one; this is achieved by taking the complex amplitude $\phi(\Omega)$ as vanishing for $\Omega < 0$. We measure the fourth-order (second-order in intensity) correlation function $\Gamma^{(2,2)}(\tau)$, which is proportional to the probability of detecting a signal photon delayed by a time τ with respect to its sibling idler. To describe the effects of spectral filtering on this correlation function, it is useful to define an effective biphoton wavepacket [25]

$$\psi(t+\tau,t) = \langle \mathrm{vac}|\hat{E}_s^{(+)}(t+\tau)\hat{E}_i^{(+)}(t)|\Psi\rangle, \tag{2}$$

where the positive-frequency field operators $\hat{E}_s^{(+)}(t+\tau)$ and $\hat{E}_i^{(+)}(t)$ are associated with annihilation of a signal photon at time $t+\tau$ and an idler at time t, respectively. The correlation function $\Gamma^{(2,2)}(\tau) = |\psi(t+\tau,t)|^2$ depends only on τ for our statistically stationary source and can be directly measured through ultrafast coincidence detection based on sum-frequency generation (SFG) [26–32], which is what we employ here. Filtering is achieved by programming complex transfer functions $H_s(\omega)$ and $H_i(\omega)$ on the signal and idler halves of the spectrum, respectively, yielding a final wavepacket

$$\psi(\tau) = \int d\Omega\, \phi(\Omega) H_s(\omega_0+\Omega) H_i(\omega_0-\Omega) e^{-i\Omega\tau}, \tag{3}$$

apart from a unimodular t-dependence and an unimportant overall scale factor. This equation governs all the results obtained below with spectral filtering.

Figure 1(a) provides the experimental setup. A continuous-wave pump beam at $\sim$774 nm is coupled into a periodically poled lithium niobate (PPLN) waveguide [33,34], generating entangled photons at 1548 nm through degenerate SPDC, with an internal efficiency of about 10^{-5} per pump photon. A typical biphoton spectrum, along with the passbands selected by the pulse shaper, is shown in Fig. 1(b) (measured on an optical spectrum analyzer at a resolution of 250 GHz). After removing the residual pump light with filters, the remaining biphotons are coupled into optical fiber and spectrally shaped by a commercial pulse shaper (Finisar WaveShaper 1000S); in all the cases examined here, a baseline quadratic phase is applied to both photons to compensate for the dispersion of the nonlinear crystals and connecting optical fiber. After leaving the pulse shaper, the photons are coupled into a second PPLN waveguide, phase-matched with the first, and recombined via SFG; at optimized dispersion compensation, the conversion efficiency is around 10^{-5} [32]. The unconverted biphotons are filtered out, and the remaining SFG photons are detected on a silicon single-photon avalanche photodiode (PicoQuant τ-SPAD) with a dark count rate less than 20 s^{-1}. Sweeping additional linear spectral-phase terms on the pulse shaper and recording the SFG counts at each step give a direct measurement of $\Gamma^{(2,2)}(\tau)$ [27]. More details of this experimental setup and high-efficiency correlator can be found in Ref. [32]. For comparison, we first show the singly peaked correlation function generated without any additional spectral modulation; the result is given in Fig. 1(c), with a full-width at half-maximum (FWHM) of about 370 fs. Each data point reflects the average of five 1-s measurements, after dark count subtraction, with dashed lines giving the theoretical result. Unless noted otherwise, the data points in all subsequent measurements of the correlation function are also averages of five 1-s measurements, with error bars giving the standard deviation and a dashed line showing the corresponding theoretical curve.

Proceeding to the case of amplitude filtering, we first note that in this method there exists a fundamental tradeoff between overall flux and the number of peaks generated. Defining ω_c as the bandwidth of a given spectral passband and ω_{FSR} as the spacing between passbands, the total number of peaks in the train is proportional to the ratio $\omega_{\mathrm{FSR}}/\omega_c$, whereas the total power transmissivity is *inversely* proportional to this quantity [35]. Combined with the fact

#206479 - $15.00 USD Received 4 Mar 2014; revised 3 Apr 2014; accepted 6 Apr 2014; published 14 Apr 2014

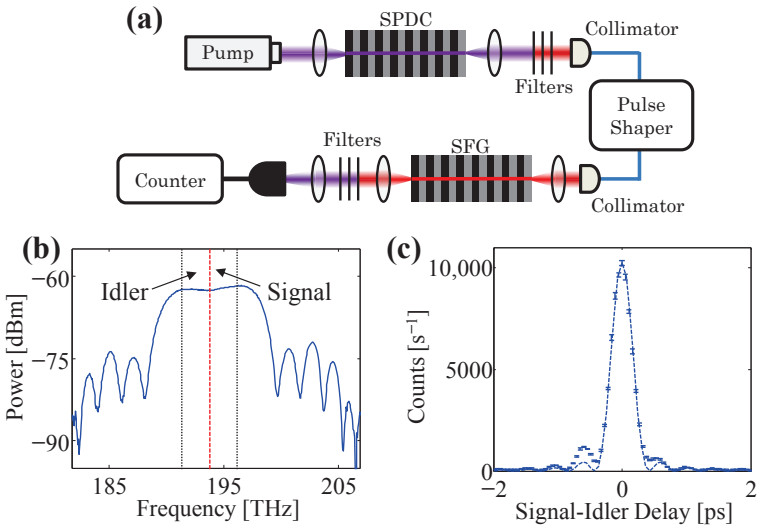

Fig. 1. (a) Experimental setup. (b) Biphoton spectrum, measured after the first collimator, with 2.4-THz signal and idler passbands marked. (c) Measured correlation function with pulse shaper compensating setup dispersion. Error bars represent the standard deviation of five 1-s measurements, and the dotted curve gives the theoretical result.

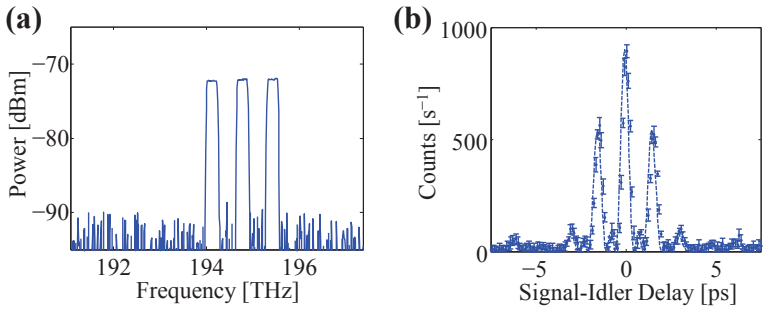

Fig. 2. Amplitude filtering. (a) Signal spectrum measured after the pulse shaper (with idler blocked). The nearly flat spectrum of Fig. 1(b) is converted to a set of three passbands, spaced by 650 GHz and each of width 250 GHz. (b) Measured temporal correlation function for the spectrum in (a), but with the low-frequency idler passed. A 650-GHz correlation train with three peaks is generated, in accordance with theoretical predictions.

that the optical energy is now distributed among many peaks, the maximum count rate actually decreases quadratically with the number of correlation peaks. Therefore to remain comfortably above the background, we program on the signal spectrum three passbands spaced at 650 GHz, each with the fractionally broad bandwidth of 250 GHz, and leave the idler untouched. The measured signal spectrum is given in Fig. 2(a), acquired with an optical spectrum analyzer at a resolution of 62.5 GHz. The spacing-to-passband ratio predicts about three temporal peaks, and this is precisely what we find for the filtered biphoton correlation function, as shown in Fig. 2(b). The result is in excellent agreement with theory, confirming the ability to produce correlation trains through straightforward amplitude filtering by our pulse shaper.

#206479 - $15.00 USD Received 4 Mar 2014; revised 3 Apr 2014; accepted 6 Apr 2014; published 14 Apr 2014

3. Biphoton temporal Talbot effect

The biphoton comb generated in the previous section lends itself well to the examination of the temporal Talbot effect. The spatial Talbot phenomenon—first reported by Henry Talbot in 1836 [36]—describes the revival of spatial interference patterns at discrete distances away from a periodic grating [37, 38], an effect which has recently been observed for entangled photons as well [39, 40]. The temporal counterpart which we consider here derives from the formal mathematical equivalence between paraxial diffraction and narrowband dispersion, known as space-time duality [41, 42]. In this dual version, a periodic electric field envelope is exactly replicated after propagation through multiples of the so-called Talbot dispersion [19, 20]. Interestingly, *fractional* Talbot dispersion can prove particularly useful and has been exploited in flattop frequency-comb generation [43, 44], repetition-rate multiplication [45–47], and high-speed temporal cloaking [48].

The origin of this effect for biphoton frequency combs can be understood most simply by considering the ideal case of a series of comb lines with infinitely narrow linewidths followed by second-order dispersion. Specifically, in Eq. (3) we take

$$H_s(\omega_0+\Omega)=\sum_{n=0}^{N-1} a_n \delta(\Omega-n\omega_{\mathrm{FSR}}) e^{i\Phi_2^{(s)}\Omega^2/2} \tag{4}$$

and

$$H_i(\omega_0-\Omega)=e^{i\Phi_2^{(i)}\Omega^2/2}, \tag{5}$$

which yields the final biphoton amplitude

$$\psi(\tau)=\sum_{n=0}^{N-1} \phi(n\omega_{\mathrm{FSR}}) a_n e^{i\Phi_+ n^2\omega_{\mathrm{FSR}}^2/2} e^{-in\omega_{\mathrm{FSR}}\tau}, \tag{6}$$

where $\Phi_+=\Phi_2^{(s)}+\Phi_2^{(i)}$, with the familiar Franson dispersion cancellation condition resulting when $\Phi_2^{(i)}=-\Phi_2^{(s)}$ [49]. As an aside, we note that the entanglement shared between signal and idler photons allows the same expression to be obtained when applying all narrowband filters on the idler instead, for it is only the *product* of signal-idler spectral filters which enters in Eq. (3). Returning to Eq. (6) we readily observe that the periodic wavepacket completely replicates itself for values of Φ_+ that are integer multiples of the Talbot dispersion Φ_T, where

$$\Phi_T=\frac{4\pi}{\omega_{\mathrm{FSR}}^2}, \tag{7}$$

as this ensures that the dispersion factor in Eq. (6) evaluates to unity for all n [18]. Taking the limit of infinitesimal linewidth for the signal spectrum shown in Fig. 2(a) gives the theoretical Talbot carpet shown in Fig. 3(a). At integer multiples of Φ_T, perfect reconstruction of the biphoton train is realized; at half-integer multiples, revivals with a half-period delay shift are obtained.

For real biphoton combs, the temporal train is not perfectly periodic, but damped by an envelope with duration inversely proportional to the non-vanishing linewidth, a well-known effect in classical pulse shaping [23]; therefore only approximate coherence revivals are possible. In particular, dispersion eventually spreads out the entire wavepacket, meaning that the self-imaging phenomenon is discernible only up to a finite multiple of Φ_T [18]. With the fractionally large linewidth in our experiments ($\omega_{\mathrm{FSR}}/\omega_c=2.6$), chosen to minimize loss, measurable Talbot interference is limited to approximately the dispersion regime $0<|\Phi_+|<\Phi_T$. This is nevertheless sufficient to observe the basic effect. Figure 3(b) presents the theoretical Talbot carpet

#206479 - $15.00 USD Received 4 Mar 2014; revised 3 Apr 2014; accepted 6 Apr 2014; published 14 Apr 2014

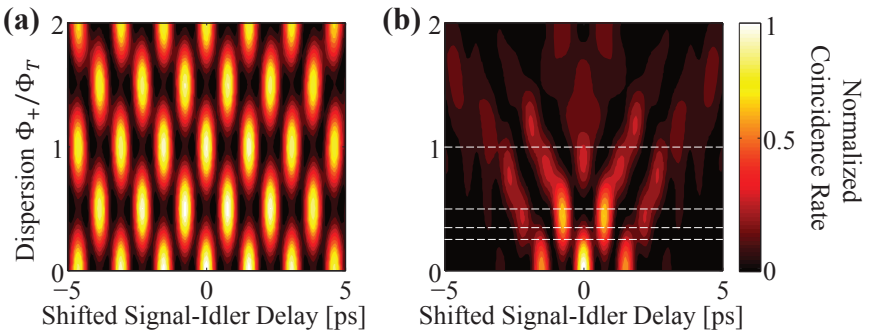

Fig. 3. Simulated Talbot carpets. (a) Theoretical temporal correlation as a function of applied dispersion, for our three-peak signal spectrum but with infinitely narrow linewidth. Perfect revivals are observed at integer multiples of the Talbot dispersion. (b) Corresponding correlation function when the linewidth is 250 GHz, as in Fig. 2(a). Dashed horizontal lines indicate the values of dispersion considered in Fig. 4. Imperfect—but still clear—self-imaging is obtained over the first Talbot length, limited by dispersive spreading. (An overall delay shift has been subtracted off for clarity.)

for our filtered biphoton source, plotting the temporal two-photon correlation function $\Gamma^{(2,2)}(\tau)$ as a function of net dispersion; horizontal lines mark the specific dispersions which we consider experimentally below. At each value of the dispersion, we have shifted the wavepacket center to zero delay, in much the same way as retarded time is calculated for classical pulses [42]. For in general, the applied dispersion introduces a frequency-dependent delay given by $\tau(\Omega) = \Phi_+\Omega$, and since the mean signal frequency offset $\langle\Omega\rangle \neq 0$, the mean signal-idler delay varies with applied dispersion. Intuitively, the fact that signal and idler are separated by frequency implies that group velocity dispersion forces them to travel at different mean speeds; therefore their average temporal separation increases as they propagate through greater amounts of dispersion.

As in the theoretical proposal of Ref. [18], we have specialized this development to the case of continuous-wave-pumped SPDC, in which the sum of signal and idler frequencies is fixed to a single value. If short-pulse pumping were considered instead, signal and idler would then be correlated about a range of frequencies, and we expect this broadened correlation bandwidth to impose an additional temporal envelope analogous to those resulting from finite filter linewidth or pulse-shaper resolution. Thus when the pump bandwidth exceeds these other characteristic frequencies, the correlation train would be severely damped. Yet for a pump whose spectrum is still narrower than the other relevant frequency scales, we expect self-imaging to nevertheless be observable. Accordingly, it would be interesting to explore the effects of such pulsed pumping in future studies—particularly the transition from the short- to long-pulse regimes—although for this first demonstration we focus on the more direct continuous-wave limit.

Experimentally, we explore the temporal Talbot effect by programming the optical dispersion directly on the pulse shaper and observing the change to the biphoton correlation function of Fig. 2(b). As before, measurement of $\Gamma^{(2,2)}(\tau)$ is made possible by applying additional, oppositely sloped linear spectral phase terms to the signal and idler spectra, to programmably control the relative delay. For our 650-GHz correlation trains, the Talbot dispersion parameter Φ_T is 0.753 ps^2, and we apply net dispersions satisfying

$$\Phi_+ = 0.25\Phi_T, 0.35\Phi_T, 0.5\Phi_T, \Phi_T. \tag{8}$$

The result for the quarter-Talbot case is presented in Fig. 4(a). The correlation train has doubled in repetition rate to 1.3 THz and matches theory well. Similar quarter-Talbot-based repetition-rate multiplication has been used to generate classical pulse trains as well [45–47]. In Fig.

#206479 - $15.00 USD Received 4 Mar 2014; revised 3 Apr 2014; accepted 6 Apr 2014; published 14 Apr 2014

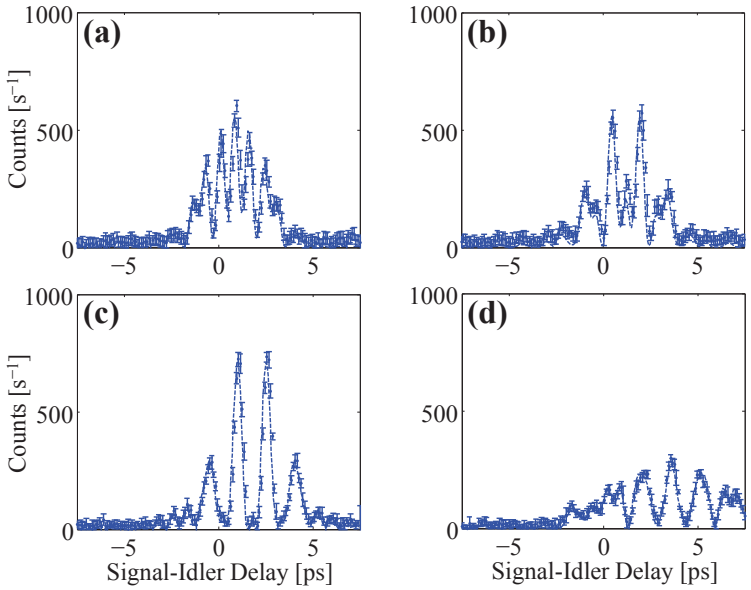

Fig. 4. Examples of Talbot interference. Biphoton correlation functions measured for dispersion Φ_+ equal to (a) $0.25\Phi_T$, (b) $0.35\Phi_T$, (c) $0.5\Phi_T$, and (d) Φ_T.

4(b), the dispersion is now 35% of the Talbot value, with the odd peaks increasing in relative magnitude and the even ones falling off, a transition which is made complete at the half-Talbot mark, as highlighted in Fig. 4(c). High-extinction peaks at 650 GHz are again clearly evident, shifted under the envelope by half a period with respect to the zero-dispersion case. Finally, the function is returned to its original state at a full Talbot dispersion [Fig. 4(d)], although the effects of finite linewidth are taking their toll as the train spreads out, resulting in a lower maximum count rate and the formation of extra satellite peaks.

For direct comparison of the coherence revivals, we numerically correct for the temporal offset due to signal-idler group velocity difference and overlay the zero-, half-, and full-Talbot correlation functions in Fig. 5(a), which clearly shows resurgence of the 650-GHz train due to temporal Talbot interference. In likewise fashion, we superpose the quarter- and zero-Talbot results in Fig. 5(b), highlighting the repetition-rate doubling. Such rate multiplication through the temporal Talbot effect is particularly advantageous in that it is achieved without removing spectral lines, which would instead reduce overall flux by an amount equal to the frequency multiplication factor [50–52]. Notwithstanding the ultrahigh efficiency of the ultrafast biphoton correlator we use [32], an obvious goal for the future would be to realize even higher detection efficiencies, which would permit demonstrations with narrower spectral filters and hence longer trains. Nonetheless, the current experiments fully confirm the theory of Ref. [18] in extending the temporal Talbot effect to biphotons.

4. Phase-only filtering

For circumstances in which the temporal biphoton phase is unimportant, and one is concerned only with the correlation function itself, an alternative method based on spectral phase-only filtering can be used to produce correlation trains much more efficiently than amplitude filtering, utilizing a technique developed early in the history of classical femtosecond pulse shaping [35] and applied to, e.g., control of molecular motion [53]. To understand this approach, consider the modulus squared of Eq. (3), where we define $K(\Omega) = \phi(\Omega)H_s(\omega_0+\Omega)H_i(\omega_0-\Omega)$ for

#206479 - $15.00 USD Received 4 Mar 2014; revised 3 Apr 2014; accepted 6 Apr 2014; published 14 Apr 2014

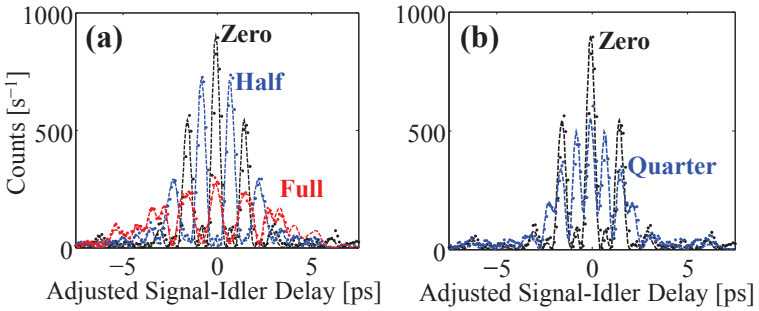

Fig. 5. Coherence revival comparison. (a) Overlay of the zero-, half-, and full-Talbot cases, after delay correction to center all at zero delay. 650-GHz trains are seen in all cases, with the finite linewidth responsible for overall spreading. (b) Overlay of the zero- and quarter-Talbot cases, again shifted so both are centered at zero delay. The original 650-GHz train is doubled to 1.3 THz at the quarter-Talbot dispersion, as expected from theory. (In both plots, error bars have been omitted for clarity.)

simplicity. This allows us to write the fourth-order correlation function as

$$\Gamma^{(2,2)}(\tau) = \int d\Omega \int d\Omega' K^*(\Omega) K(\Omega') e^{i(\Omega-\Omega')\tau}. \tag{9}$$

Redefining a new integration variable Δ according to $\Delta = \Omega' - \Omega$ and replacing Ω' gives

$$\Gamma^{(2,2)}(\tau) = \int d\Delta e^{-i\Delta\tau} \int d\Omega K^*(\Omega) K(\Omega+\Delta). \tag{10}$$

Thus the measured correlation function is given by the inverse Fourier transform of the autocorrelation of the filtered biphoton spectrum, and so the condition for a periodic train requires only that this *autocorrelation* consist of discrete peaks—$K(\Omega)$ itself need not be comb-like. In our case, we achieve the desired spectral peaks by taking $H_i(\omega) = 1$ and choosing $H_s(\omega)$ to be a periodic repetition of a maximal-length binary phase sequence (M-sequence) [54], which indeed possesses discrete spikes in its autocorrelation. Since the input biphoton spectrum is essentially flat over the pulse-shaper passband, no additional amplitude equalization is required, and so the spectral filtering is ideally lossless. In stark contrast to the amplitude filtering of Sec. 2, the maximum count rate drops only linearly with the number of peaks generated by phase filtering—instead of quadratically—thereby offering the potential for significantly longer biphoton trains at a given flux. However, we emphasize that temporal interference effects, such as the Talbot phenomenon, do not carry over to these non-comb-like states, since the inter-peak temporal phase varies widely.

We first consider the length-7 M-sequence [0 1 1 1 0 1 0], where we map the zeros to phase 0 and the ones to phase π. Each element is programmed to cover a bandwidth of 115 GHz, giving a total of three repetitions of the M-sequence over the 2.415-THz signal passband set on the pulse shaper here. The measured correlation train is presented in Fig. 6(a), again showing good agreement with theory. The missing peak at zero delay results from destructive interference between the 0- and π-phase elements. We can restore the central peak by changing the binary phase shift; taking 0.78π for the shift instead of the original π, we obtain the blue curve in Fig. 6(b). A high-contrast train at 805 GHz is generated under a smooth envelope, without any amplitude filtering of the biphoton spectrum.

To directly compare the flux improvement over the equivalent amplitude filter, we also program three repetitions of the amplitude sequence [1 0 0 0 0 0 0] over the same bandwidth,

#206479 - $15.00 USD Received 4 Mar 2014; revised 3 Apr 2014; accepted 6 Apr 2014; published 14 Apr 2014

which gives the desired 805-GHz train but at the cost of removing much of the original biphoton spectrum. This result (red curve) is compared to the phase-only approach in Fig. 6(b); the amplitude case is reduced approximately 7-fold in integrated flux and is barely visible above the noise. We run a similar comparison for length-3 sequences as well, giving each symbol a bandwidth of 160 GHz and replicating the sequence five times over a 2.4-THz total signal bandwidth. For the phase filter, we use the M-sequence [1 0 1], where ones now map to a phase shift of 0.65π; for the amplitude filter, we take the transmission sequence of [1 0 0]. Both results are compared in Fig. 6(c), and a count rate improvement of about 3:1 is observed for the phase-only sequence. These results stress the substantial flux increases facilitated by pure phase filtering, which—coupled with the programmable control of peak number and spacing—make such states valuable tools for future work with high-repetition-rate biphotons.

5. Resolution limitations

In Sec. 2, we discussed the flux reduction resulting from periodic amplitude filtering of the broadband biphoton spectrum, showing in Sec. 4 how this can be mitigated through phase-only filtering. Here we confront and analyze a separate restriction imposed by the finite pulse-shaper resolution: time aperture. The time aperture, or the maximum temporal duration over which the shaped waveform will accurately reproduce that of the ideal infinite-resolution mask, is fixed by the resolvable frequency spacing [21–23]. If we model this temporal window as a Gaussian function with an intensity FWHM $T_{\mathrm{FWHM}} = (2\ln 2)^{1/2}T$, the effect of finite resolution is to

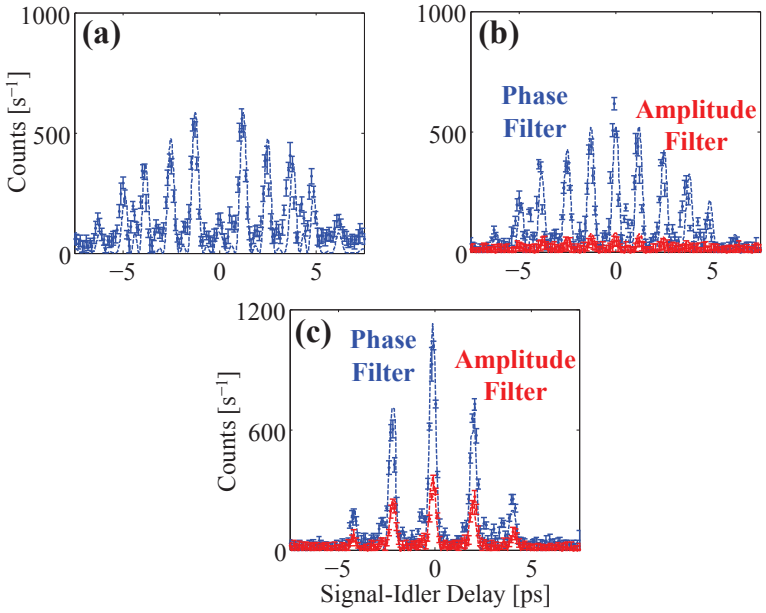

Fig. 6. M-sequence filtering. (a) Measured correlation function for length-7 M-sequence with a π phase shift. (b) Correlation function for the same M-sequence but with a 0.78π phase shift (blue), compared to an amplitude filter at the same repetition rate (red). (c) Correlation function for a length-3 M-sequence with a 0.65π phase shift (blue) and the corresponding amplitude filter. In both (b) and (c), phase filtering yields a flux improvement roughly equal to the number of peaks.

#206479 - $15.00 USD Received 4 Mar 2014; revised 3 Apr 2014; accepted 6 Apr 2014; published 14 Apr 2014

yield the impulse response $h(t)$ (the inverse Fourier transform of the transfer function $H(\omega)$)

$$h(t) = h^{(0)}(t)e^{-t^2/T^2}, \tag{11}$$

where $h^{(0)}(t)$ is the impulse response corresponding to an infinite-resolution pulse shaper. Therefore the generated trains are restricted to a time window roughly equal to the inverse of the spectral resolution. Now when the characteristic frequency scale $\delta\omega$ over which the ideal mask $H^{(0)}(\omega)$ varies satisfies $1/\delta\omega \ll T$, $h(t) \approx h^{(0)}(t)$, and the effects of finite resolution are negligible (which was the case in the previous sections). However, to explicitly examine the limits of our biphoton correlation train generator, now we choose filter functions that are significantly modified by the time aperture. Moreover, because we use the pulse shaper not only for generation but also for imposing the relative signal-idler delay, we suffer on two counts: first in the creation of the correlation train, and second in its measurement. Letting $\tilde{\psi}(\tau)$ denote the measured wavepacket under the effects of finite pulse-shaper resolution, to best reflect the experimental conditions of our measurement, the expression in Eq. (3) must be modified to

$$\tilde{\psi}(\tau) = \int d\Omega\, \phi(\Omega)\tilde{H}_s(\omega_0 + \Omega, \tau/2)\tilde{H}_i(\omega_0 - \Omega, -\tau/2), \tag{12}$$

where the delay τ is explicitly imposed by the filters, with the signal temporally shifted by $\tau/2$ and the idler by $-\tau/2$ [27]. The corresponding infinite-resolution filters are thus

$$\tilde{H}_s^{(0)}(\omega_0 + \Omega, \tau/2) = C(\Omega)e^{-i\Omega\tau/2} \tag{13}$$

and

$$\tilde{H}_i^{(0)}(\omega_0 - \Omega, -\tau/2) = e^{-i\Omega\tau/2}, \tag{14}$$

where $C(\Omega)$ is the ideal spectral code applied to the signal photon. The finite-resolution filters $\tilde{H}_s(\omega, \tau)$ and $\tilde{H}_i(\omega, \tau)$ are obtained by convolving $\tilde{H}_s^{(0)}(\omega, \tau)$ and $\tilde{H}_i^{(0)}(\omega, \tau)$ with the Fourier transform of the time aperture function e^{-t^2/T^2}. In this way we can incorporate the effect of finite resolution on both the spectral code and imposition of signal-idler delay.

Experimentally, we take the same periodically repeated length-3 phase sequence as in Sec. 4, but this time consider very narrow spectral chips. In order to correct for count-rate reduction due to alignment drift, we normalize each correlation function to a peak value of unity; since the time aperture term is equal to one at zero signal-idler delay, such renormalization has no effect on examination of aperture effects. In the first case, we program a chip bandwidth of 16 GHz, for a total of 50 repetitions of the fundamental sequence over the 2.4-THz signal bandwidth; the measured correlation function is given in Fig. 7(a). Compared to the 160-GHz chip case in Fig. 6(c), the peak separation has been pushed from 2.1 to 21 ps, and the two side peaks are lowered slightly in relative intensity by the pulse-shaper time aperture. Further reductions are evident for even smaller chips; Fig. 7(b) shows the results for 9-GHz chips (total signal bandwidth 2.403 THz), and Fig. 7(c) those for 5-GHz chips (2.4-THz total signal bandwidth). We find that a value for T of 50 ps ($T_{\mathrm{FWHM}} = 58.9$ ps) gives good agreement with the observed peak reduction, as evident by the dotted theoretical curves in Fig. 7. This experimentally measured time aperture corresponds to a 3-dB spectral resolution of about 7.5 GHz, slightly better than the 10 GHz specified for the WaveShaper 1000S. From these results, it is clear that pulse-shaper resolution limits the overall duration of the generated biphoton correlation function to a window of around 50 ps. Any slower detection schemes are therefore unable to resolve these correlation trains, so while this phase-only filtering method is well suited for programmable generation of high-repetition-rate biphoton trains, the narrow linewidth available from resonant photon-pair generation [2–5, 9, 10, 15–17] or filtering with an etalon [7, 8] would prove more appropriate when temporally long trains are required.

#206479 - $15.00 USD Received 4 Mar 2014; revised 3 Apr 2014; accepted 6 Apr 2014; published 14 Apr 2014

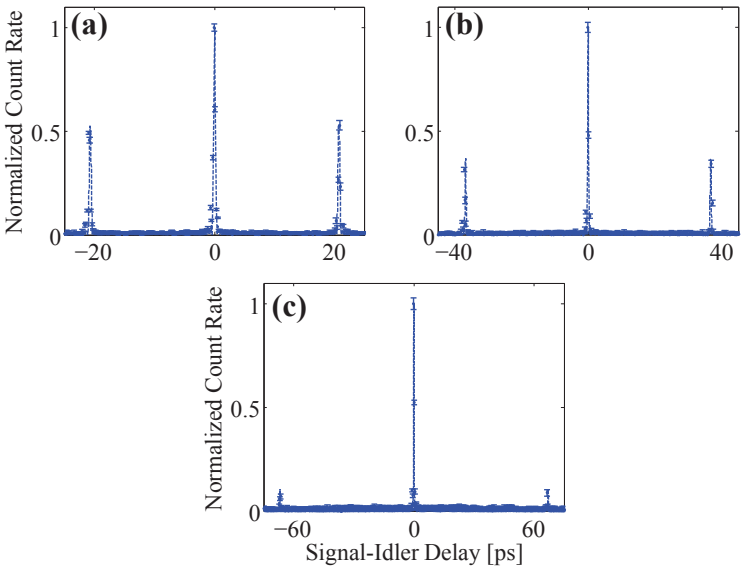

Fig. 7. Examination of pulse-shaper time aperture. Normalized coincidence rate for periodic repetitions of length-3 M-sequences with (a) 16-GHz chips, (b) 9-GHz chips, and (c) 5-GHz chips. The theoretical curves are obtained with $T = 50$ ps in Eq. (11).

6. Conclusion

We have experimentally implemented several techniques based on programmable spectral filtering for the generation of biphoton correlation trains. Amplitude filtering was first used to create an approximately comb-like spectrum, and accompanying this filter with appropriate quadratic spectral phase, we were able to demonstrate for the first time coherence revivals and repetition-rate multiplication through the biphoton temporal Talbot effect. Subsequently we explored phase-only filtering to generate correlation trains with much greater efficiency over the amplitude filtering approach, useful when the temporal biphoton phase is of no concern. Finally, by pushing the inter-peak separation to long delays, we verified the time aperture limits imposed on our technique by finite pulse-shaper resolution. Overall, these demonstrated spectral filtering tactics could prove quite valuable in future work on periodic biphotons, particularly where high speeds and tunability are advantageous. We are curious how applications similar to those explored with classical pulses, such as selective molecular excitation [53], may benefit in interactions at the quantum level from the repetitive biphotons obtained here.

Acknowledgments

This work was supported by the Office of Naval Research under Grant No. N000141210488. J.M.L. acknowledges funding from the Department of Defense through a National Defense Science and Engineering Graduate Fellowship.